Renewable Energy 257 (2026) 124805

Contents lists available at ScienceDirect

Renewable Energy

journal homepage: www.elsevier.com/locate/renene

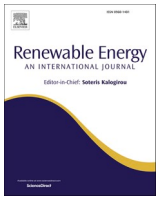

Geothermal plant operation and control under demand uncertainties

Pejman Shoeibi Omrani [a,b,*], Paul J.P. Egberts [b], Huub H.M. Rijnaarts [a,c], Shahab Shariat Torbaghan [a]

[a] Environmental Technology, Wageningen University & Research, Bornse Weilanden, Wageningen, the Netherlands
[b] Heat Transfer and Fluid Dynamics Department, TNO, Kesslerpark 1, Rijswijk, the Netherlands
[c] Institute for circular society of the EWUU alliance: Universities of Eindhoven, Wageningen, Utrecht and University Medical Centre Utrecht, the Netherlands

ARTICLE INFO

Keywords:
Robust optimization
Geothermal production and operation
Decision support systems
Uncertainty
Genetic algorithm

ABSTRACT

Geothermal energy plant operations are significantly influenced by uncertainties in key parameters and processes, including the variability heating demand in the built environment compared to the more stable demand in horticulture, necessitating a robust framework for real-time decision-making. This paper introduces a novel robust optimization framework to enhance geothermal plant performance under uncertain heating demand. The proposed method integrates a genetic algorithm with a geothermal plant simulator, optimizing dual objectives: emission reduction and profit maximization. Operational constraints are incorporated via penalties in the objective function. The approach identifies distinct control strategies for each objective, effectively capturing varying operational behaviors and demonstrating adaptability to different performance goals. Results from the numerical case study indicate that, under the considered modelling assumptions, robust optimization delivers more resilient and effective control strategies across all considered realizations of uncertain heat demand compared to deterministic optimization. For a fixed daily heat demand, the robust approach achieved a 5.9 % reduction in emissions and a 1.4 % increase in profit compared to the best deterministic scenario. These findings underscore the potential of robust optimization in addressing uncertainties and improving the operational efficiency of geothermal energy plants.

1. Introduction

Geothermal energy plays an increasingly important role in the energy transition and offers a sustainable and reliable solution for decarbonizing heating and cooling in buildings, industrial processes, and agriculture [1]. Its widespread availability beneath the Earth's surface makes it a promising alternative to fossil fuels, with the potential to significantly reduce greenhouse gas emissions. The deployment of geothermal energy faces challenges such as high upfront costs, integration into heating and cooling networks, and operational challenges which currently supply less than 2 % of Europe's demand [2,3]. Despite an extensive operational experience in geothermal plants, characterized by a steep learning curve with ongoing operational knowledge acquisition, the sector is still in an emerging phase. The operation of geothermal plants is often associated with several challenges caused by the complex geothermal production behavior [4] and geothermal fluid compositions [5]. Operators require support to make effective decisions in managing geothermal plants, as complex fluid compositions and reservoir behaviors demand continuous monitoring and precise adjustments. Decision-support tools and predictive models can assist operators by providing insights into optimal operational strategies, helping to maintain system stability and maximize energy production under varying conditions.

Uncertainties in geothermal operation significantly impact the efficiency, reliability, and economic feasibility of the energy system [6,7]. These uncertainties arise from various sources, including unpredictable geological and reservoir conditions [8], variations in geothermal fluid composition [9], and performance of equipment [10]. Such factors can alter the thermal output and energy yield, challenging operators to maintain optimal performance. Additionally, uncertainties in demand and energy prices add layers of complexity to operational planning. One of the main goals of the geothermal plant operation is to supply the heat demand efficiently and sustainably either to the greenhouses, buildings or districts. The daily and seasonal variability in the heat demand [11]

This article is part of a special issue entitled: Geothermal heating-cooling published in Renewable Energy.

* Corresponding author. Environmental Technology, Wageningen University & Research, Bornse Weilanden, Wageningen, the Netherlands.
E-mail address: pejman.shoeibiomrani@tno.nl (P. Shoeibi Omrani).

https://doi.org/10.1016/j.renene.2025.124805
Received 17 December 2024; Received in revised form 10 August 2025; Accepted 20 November 2025
Available online 21 November 2025

can impose more challenges to the operational and production decisions in the geothermal plants. In the context of built environment, next to the variability of the heat demand, the uncertainties in the heat demand can have a large impact on the operational excellence [12,13] and CO_2 footprint of the energy supply. This unpredictability necessitates robust strategies to optimize system performance under uncertain conditions, such as adaptive controls, predictive maintenance, and scenario-based planning, ensuring that geothermal systems remain cost-effective and resilient while maximizing energy extraction.

Optimization methods can be used to maximize the geothermal production performance by optimizing different types of decision and control variables such as the change in the geothermal production and the use of auxiliary components while adhering to operational constraints [14]. Due to the presence of various control parameters and constraints, this results in a high-dimensional, non-convex, and constrained optimization problem. In addition, the optimization process should be conducted with consideration of the inherent uncertainties that arise from the limited knowledge on the variability of the processes and heat demand.

These uncertainties can impact design and operational decisions in the geothermal plants. Such practices are broadly studied and demonstrated in the petroleum industry [15,16] and started to get more attention in the geothermal industry. We have performed a literature review to survey available studies in the geothermal plants for design and operation optimization. For such a literature survey, the ground source heat pump systems were excluded due to the difference in the type and mechanisms of these systems, scale, and interaction with geothermal reservoirs. In addition, the literature for both direct-use and power production applications were collected. A summary of the available literature, up to current date, can be found in Table 1.

One of the initial findings was that most current studies and literature focus on using optimization for the design and operation of geothermal plants dedicated to power production. Recently, a few studies have also addressed optimization under uncertainties for the design of both direct-use and power production geothermal plants. Additionally, long-term production strategies under uncertainty in geothermal plants have been explored [7,17]. However, to the authors knowledge, no studies to date have examined the operational optimization of direct-use geothermal plants under uncertainties.

This paper aims to highlight the impact of demand uncertainties on the operation and control of geothermal plants for direct-use (heating) applications which have not be studied in literature. Its primary contribution lies in demonstrating a robust optimization approach for controlling geothermal plants with various operational strategies and objectives under uncertainty. The paper is organized as follows: first, the case study is introduced, including a description of the numerical simulator (details provided in Annex 1). Next, the mathematical optimization problem is formulated, encompassing objective functions, constraints, and the employed optimization algorithm, which is applied to the case study. Subsequently, the results of the robust optimization for different objective functions are presented and discussed. Finally, the paper concludes with key findings and suggestions for future research. To the best of the authors' knowledge, this is the first study to address uncertainty in the control and optimization of geothermal plants for short-term operational decisions. The methods proposed in this study are considered novel in this context.

Table 1
List of available literature for employing numerical optimization for the design and operation of geothermal plants for both direct-use (heating) and power production applications, note that ground-source heat pumps were excluded from the overview.

Reference	Application		Phase		Uncertainty
	Direct-use	Power	Design/ Planning	Operation	
[18]; [19]; [20]; [21]; [22]; [23]; [14]	×	✓	✓	×	×
[24]	×	✓	✓	✓	×
[25]; [26]; [27]; [28]; [29]; [30]; [31];	×	✓	×	✓	×
[6]; [32]	×	✓	✓	×	✓
[33]; [34]; [35]	✓	×	✓	×	✓
[17]; [7]	×	✓	×	✓	✓
[36]	✓	✓	×	✓	×
[37]	✓	×	×	✓	×

2. Physical system modeling assumption

In order to demonstrate the optimization under uncertainty on the operational decisions of geothermal plants, an example of low-enthalpy hydrothermal geothermal plant was selected. The schematic of a geothermal plant which is used in this study is shown in Fig. 1. Each geothermal plant can have different components and equipment; in Fig. 1 a relatively detailed geothermal plant is sketched which was inspired by a real geothermal plant in the Netherlands. The geothermal plant consists of a primary system and the secondary system. The different components in the primary side of the geothermal plant contain the geothermal wells (producer: hot side and injector: cold side), gas-liquid separator, filters, heat exchangers, electrical submersible pump (ESP) and injection booster pump. On the secondary side, different auxiliary equipment such as a gas dryer, gas boiler and a combined heat and power (CHP) unit is installed.

In the primary system, the geothermal production facility consisted of a producer and an injector well. In this paper, the reservoir pressure is considered to be 240 bars with the productivity index (PI) of 10 m3/(bar.h). The wells are vertical and have the depth of 2000 m (the Dutch geothermal gradient varies between 31 and 35 °C/km) which enables the production temperature of 70–80 °C. The geothermal brine has a high salt content of 200 kppm (NaCl equivalent) with an assumed density of 1180 kg/m^3, the specific heat capacity of 4.2 kJ/(kg.C), dynamic viscosity of 0.35 mPa s and the temperature dependency of the fluid properties is not considered in this case study. The geothermal fluid is produced with associated gas with a gas-liquid ratio of 0.5 Nm^3/m^3, (N denotes the normal condition at the temperature of 0 °C and pressure of 101.325 kPa). The majority of the produced gas is assumed to be methane and CO_2. The actual volume of the produced gas will depend on the production rate and the wellhead pressure. Most of the Dutch wells are being operated at a slightly elevated pressures to keep the CO_2 dissolved in the brine solution and minimize the calcium carbonate scaling [38]. Geothermal fluid is being produced in production well assisted by an ESP. The ESP installation depth of 650 m and the tubing size of 0.15 m. A gas-liquid separator is installed to separate the by-produced gas from the brine and control the top-side pressure of the geothermal well. The brine will go through a set of filters, and then a heat exchanger to transfer the heat from the geothermal brine to the secondary side of the plant. The colder brine will be injected into the geothermal reservoir through an injector well.

On the secondary side, the separated gas will be dried and will be fed

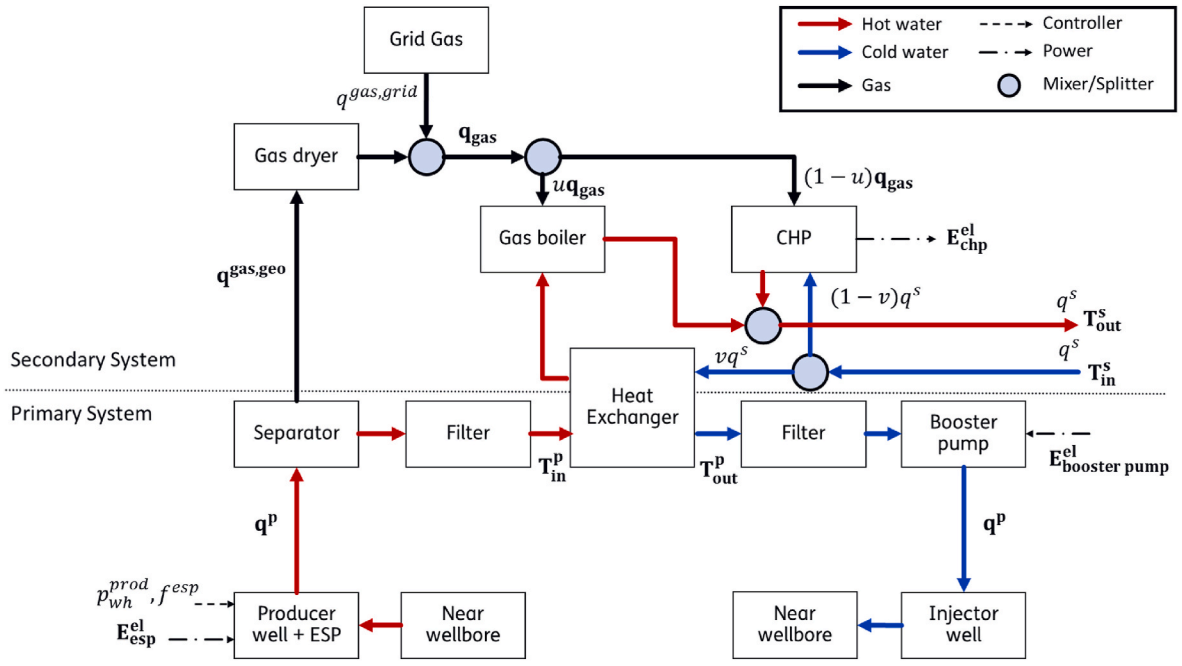

Fig. 1. Schematic of the geothermal plant and its components including both primary and secondary systems.

into the gas boiler or a CHP unit for providing additional heat and power. The additional heat can be combined with the thermal energy extracted from the geothermal brine to be supplied to the demand side (district heating grid, space heating or a greenhouse). The additional power generated in a CHP can be used to power the electrical equipment in the geothermal plant, such as ESP and injection pumps. The CHP, in this case, will work with the produced gas from the geothermal doublet, denoted by $q^{gas,geo}$, and additional gas which can be taken from the gas grid, denoted by $q^{gas,grid}$. Part of the total gas (q_{gas}) will be fed into the boiler (uq_{gas}) and the rest will be fed to the CHP unit $\left((1-u)\,q_{gas}\right)$, see Fig. 1. In addition to delivering electricity to pumps the CHP may heat a part of the cooled down fluid stream q^s that is divided among the CHP ($(1-v)q^s$) and the Heat exchanger (vq^s). The fractions u and v are control variables of which its values to be derived so to maximize a chosen objective. Other control variables of the plant are the ESP frequency f^{esp}, the producer's well head p^{prod}_{wh}, the amount of gas $q^{gas,grid}$ taken from the gas grid, and q^s which is the flow rate of the fluid in the secondary system. The parallel integration of geothermal heat and CHP in this case study reflects actual configurations observed at operational sites for which process data were available. While a series connection at the highest temperature could be more optimal from an exergetic perspective, the chosen setup ensures the case study remains representative of a real-world layout.

An in-house developed solver was used for solving the primary and secondary system in the example geothermal plant. Since, the production in the primary system of geothermal plants is pressure driven, the solver is based on nodal analysis. Nodal analysis is a systematic method used for subsurface production systems to simulate and optimize production systems by evaluating inflow and outflow across each component, from reservoir to surface equipment with a broad application area from well performance prediction to artificial lift design to equipment sizing [39].

To briefly explain the steps used by solver to simulate the geothermal plant;

1) Determine the flow rate q^p of the primary system using nodal analysis between the producer well, ESP and near wellbore (reservoir). This calculation involves the components describing vertical lift performance (VLP) of the producer, ESP and inflow performance relation (IPR) of the aquifer.
2) Calculate all downstream components and nodal pressures for the primary system. The bottom hole and wellhead pressures of the injector is calculated give the flowrate q^p calculated through the IPR and the injector's VLP.
3) Calculate the intake temperature T^p_{in} of the heat exchanger at the primary system given a measured temperature, in this case the reservoir temperature (no heat loss is assumed in the geothermal plant)
4) Calculate the discharge temperatures T^p_{out} and T^s_{out} with input T^p_{in}, T^s_{in} and the flow rate q^s of the secondary system.
5) Calculate the downstream temperatures of the system using T^p_{out} and T^s_{out}, calculated in 5. Auxiliary components in the secondary side, will provide additional heat or power based on the proposed control settings (meaning the value of the control variables used in a model evaluation).

The solver is written in python, the nodal analysis resulting in a root-finding problem for the flowrate q^p is solved through a bisection method using the root_scalar method from the scipy.optimize python library. A detailed description of the models used for different components can be found in the Annex section. In addition, a detailed description of the solver and the model is presented by Ref. [37].

For the primary side of the geothermal plant, except for the wells, no pressure loss is considered. The plant components, e.g. filter, heat exchanger, separator, CHP and boiler are simulated using fast-to-evaluate steady-state models (further explained in Annex 1). For the filter and separator model, a pressure and temperature drop between intake and discharge can be provided. For the heat exchanger a steady-state counterflow model is used based on the NTU-method. The boiler model sets the water heat rate equals to the power generated by the gas fuel with an efficiency factor (assumed to be 0.8). For the CHP model we assume that 1/3 of the power generated by the fuel is converted to electricity and the remaining power is used for the heat generation. The calorific value of the gas entering the boiler and/or CHP is 50 MJ/kg.

3. Methodology

In this section the methodology of the problem is described. Fig. 2 illustrates the workflow of the proposed optimization framework for the geothermal plant operation under demand uncertainty. This flowchart provides a visual representation of the sequential steps involved in our framework, facilitating a comprehensive understanding of its operation. The process initiates with the definition of initial control settings and a geothermal plant model. Separately, the demand uncertainty needs to be defined in terms of its probability distribution function or any description that can be used by the optimization algorithm for the propagation and evaluation of these uncertainties. Based on the initial or proposed control settings, the objective function is evaluated over all possible demand realizations, and the corresponding objective values are obtained. These values are then utilized by the optimization algorithm to determine optimal control strategies. The process iterates until the termination criteria are met, at which point the final optimal results are determined.

Mathematically, the control problem is formulated as a two-stage scenario-based stochastic optimization (SBSO) problem. In this framework, the decisions in the first stage correspond to the "here and now" decisions, which are common across all scenarios. In contrast, the decisions in the second stage are "wait-and-see" decisions, optimized for each individual scenario. A standard approach in SBSO for a risk-neutral decision-maker is to optimize the expected value of the objective function, averaged across all scenarios [40].

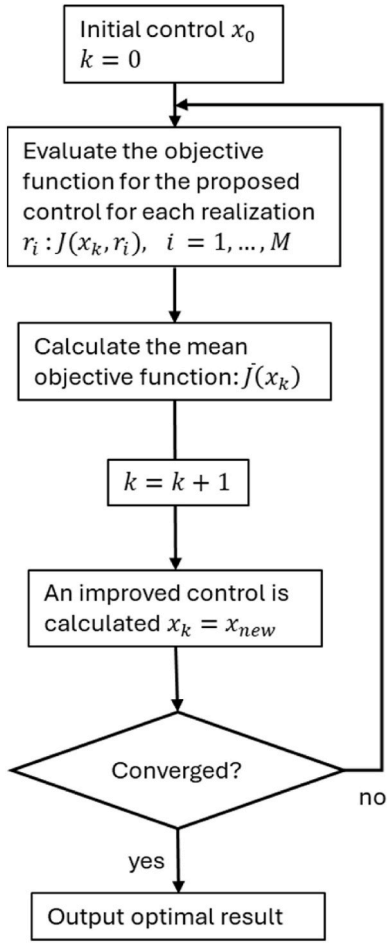

Fig. 2. Schematic of the optimization workflow. It starts with an initial guess x_0 of the control. In an iterative process the optimizer calculates improved control until the objective function improvement is below a tolerance $\epsilon > 0, i.e.\ |\bar{J}(x_k) - \bar{J}(x_{k-1})|/\bar{J}(x_{k-1}) < \epsilon$.

SBSO serves as a general framework that accommodates various risk-handling strategies. In a risk-neutral setting, the objective function is typically formulated to optimize the expected value across all scenarios [42]. Alternatively, risk-averse approaches include chance-constrained, CVaR-based, or robust optimization formulations [41], depending on how uncertainty is treated in the objective and constraints.

In this study, we adopt a robust optimization strategy within the SBSO framework. Specifically, the control problem is solved by identifying a single set of control variables that performs best under the worst-case scenario among all considered realizations of the uncertain heat demand. This approach yields a solution that is robust, meaning it ensures system performance even under the most adverse demand conditions but can be suboptimal for every individual realization [16,42,43]. Due to the specific nature of the geothermal case study, no first-stage (pre-commitment) decisions are required in advance, allowing for the decoupling of the problem across scenarios. As such, the optimization focuses solely on second-stage decisions, control set-points that directly affect system operation.

In the following sections, the optimization problem, objective function, and associated constraints are described. The optimization algorithm returns optimized control values for adjusting the operation of the geothermal plant (so called the control set-points) that optimizes the chosen objective function. Key performance indicators (KPIs) are evaluated for the plant operated using these control set-points. Following the description of the optimization problem, the formulation of the optimization problem under uncertainty, using SBSO, is provided. Finally, the optimization algorithm, its parameters, and termination criteria are presented.

3.1. Optimization problem

In the operation of a geothermal doublet plant, the objective may be to maximize profits and/or minimize emissions while adhering to operational constraints. In the present case study, a total of six control variables are considered, which already presents significant challenges for manual optimization. This section formalizes the optimization problem. Prior to this, a list of global key performance indicators (KPIs) for the example plant, which are subject to optimization, is presented. These KPIs are computed by the simulation model for each proposed control action. In the description of the KPIs below, the superscript "el" denotes electric power, while "s''refers to variables in the secondary system, as shown in Fig. 1.

The KPI's related to power [MW] are:

- $E_{plant} = q^s \rho C_w \left(T^s_{out} - T^s_{in}\right)$ represents the thermal power generated by the plant, where
  - o C_w: specific heat capacity of water [J/(kg K)],
  - o ρ: water density [kg/cm^3],
  - o q^s: flow rate [m^3/s],
  - o T^s_{out}: outlet temperature of the secondary system [K],
  - o T^s_{in}: inlet temperature of the secondary system [K]
- $E_{total} = E_{plant} - E^{el}_{esp} - E^{el}_{boosterpump} + E^{el}_{chp}$, represents the net generated power. This accounts for power consumption of pumps and power generation by the CHP component.
- $E^{el}_{net} = -E^{el}_{esp} - E^{el}_{boosterpump} + E^{el}_{chp}$, represents the electricity surplus. If non-negative, the CHP can supply all electricity required for the plant.

The total emission KPI [kg/h of CO_2 equivalent]:

- $M_{total} = M_{esp} + M_{boosterpump} + M_{boiler} + M_{chp}$, represents the total CO_2 emission.

To calculate the emission terms for the pumps (ESP and booster pump), their power consumption is determined based on the pump head

and flow rate, along with an emission factor associated with the power source. The emission terms for the boiler and CHP are based on the amount of natural gas consumed by these components. Detailed formulations for these emissions are provided in the component modeling Annex 1.

The total profit KPI [€]:

- $C_{total} = c_{heat}E_{plant}(x) - c_{el}E^{el}_{net}(x) - c_{CO_2}M_{total}(x) - c_{gas}q^{gas,grid}$ represents the total costs, where
  - o c_{heat}: price of the heat [€/GJ]
  - o c_{CO_2}: price of CO2 [€/tonne]
  - o c_{gas}: price of the gas [€/MMBtu]
  - o c_{el}: price of the electricity [€/MWh]

A geothermal plant has several control variables, which, for the case study example, are identified as follows:

- Wellhead pressure of the producer p^{prod}_{wh}
- ESP frequency f^{esp}
- Flow rate of gas from the grid $q^{gas,grid}$
- Gas flow fraction $u \in [0,1]$
- Water flow fraction $v \in [0,1]$ of the secondary system
- Flow rate q^s at secondary system

To simplify, these control variables are grouped in a control vector x defined by:

$$x = \left(f^{esp}, p^{prod}_{wh}, q^{gas,grid}, q^s, u, v\right). \tag{1}$$

The feasible control space, defined by the control variable upper and lower bounds, is denoted by Ω.

We consider two KPI's for optimization: minimizing the total emission M_{total} and maximizing the total profit C_{total}. Both optimization problems are formulated as follows:

$$\left\{\min_{x\in\Omega} J(x) \mid h(x) = 0, g(x) \le 0\right\}, \tag{2}$$

where objective function J defined by $J(x) = M_{total}(x)$ for emission minimization and $J(x) = -C_{total}(x)$ for profit maximization (note that maximizing profit (C_{total}) is equivalent to minimizing $-\ C_{total}$).

The constraints are expressed in vector notation as follows:

$h = 0$: equality constraints $h_i(x) = 0, i = 1,\ldots,m$,
$g \le 0$: inequality constraints $g_i(x) = 0, i = 1,\ldots,n$

Here, m and n denote the number of equality and inequality constraints, respectively. Specific constraints used in the study include:

- A minimum outlet temperature for the secondary system, $T^s_{out} \ge T^{min}_{out}$
- A constraint on the wellhead pressure to prevent scaling and mineral precipitation, $p^{prod}_{wh} > p_{scaling}$.

For the case study example, $p_{scaling}$ and T^{min}_{out} are set to 4 bars and 50 °C, respectively.

3.2. Optimization under uncertainty

In a geothermal plant, there are several sources of uncertainty arising from different origins, such as the properties of the fluid and reservoir, as well as the variability in energy demand. In our modeling approach, for instance, uncertainty in reservoir properties is reflected in the productivity index (PI) of the inflow performance relation. With deterministic optimization, fixed values are assigned to uncertain parameters, and the optimization problem is solved as described in the previous section. This approach provides an optimal control strategy based on somewhat arbitrary parameter values. Ideally, the resulting optimal control should be tested to evaluate its performance across other realizations of the uncertain parameters. However, this workflow is cumbersome and does not guarantee an acceptable solution. The stochastic optimization framework outlined above, including both SBSO and robust optimization methods, addresses this issue. It aims to identify a control policy that performs well across all realizations of the uncertain parameters. Robust optimization methods, in particular, ensure feasibility under all possible realizations of the uncertain parameters by considering their worst-case scenarios [35,44].

To outline the stochastic optimization approach, we assume that uncertainties are represented by a set of realizations $r = (r_1, r_2, \ldots, r_m)$ with the associated probabilities $\omega = (\omega_1, \omega_2, \ldots, \omega_M)$, where the probabilities satisfy $\sum_{i=1}^{M}\omega_i = 1$. For equiprobable realizations $\omega_i = 1/M$, $i = 1,\ldots,M$.

The evaluation of the objective function J, as described above, depends not only on the control vector x but also on a chosen realization, say r_i. The expected value of the objective function can then be written as:

$$\bar{J}(x) = \sum_{i=1}^{M}\omega_i \,.\, J(x, r_i) \tag{3}$$

The stochastic optimization framework focuses on maximizing the expected objective function value $\bar{J}(x)$, as opposed to optimizing $J(x, r_i)$ for a single arbitrary realization r_i, as is done in deterministic optimization. As outlined above, in the case of SBSO, the optimal control policy is determined for each scenario by optimizing the expected objective value across all scenarios. This approach differs from focusing on a single solution that performs best under the worst-case scenario. While this approach ensures feasibility and conservatism, it can lead to suboptimal performance in scenarios other than the worst case, thereby sacrificing some efficiency in favor of robustness. When heat demand is considered as one of the uncertainties, the objective function (per scenario) $J(x, r_i)$ is augmented with a penalty term to account for the mismatch between the heat supplied (E_{plant}) and the heat demand (E_{demand}). For the emission minimization case, the augmented objective function takes the form:

$$J(x, r_i) = M_{total}(x, r_i) + \mathscr{P}(x, r_i) \tag{4}$$

Where $\mathscr{P}$ denotes the penalty term for constraint violations. For the case study presented in this paper, the constraint violation term is expressed as:

$$\mathscr{P}(x, r_i) = c_1 \left\| E_{plant}(x, r_i) - E_{demand}(r_i) \right\| + \begin{cases} c_2, & \text{if } p^{prod}_{wh} \le p_{scaling} \\ 0, & \text{otherwise} \end{cases} + \begin{cases} c_3, & \text{if } T^s_{out} < T^{min}_{out} \\ 0, & \text{otherwise} \end{cases} \tag{5}$$

where $\|\cdot\|$ is the Euclidian norm, $c_1, c_2, c_3 > 0$ are penalty factors and $E_{demand}(r_i)$ is the demand profile associated to realization r_i. Likewise, for the profit optimization $M_{total}(x, r_i)$ is replaced by $-C_{total}(x, r_i)$. Penalty factors are introduced in the objective function to enforce key operational constraints, such as temperature limits, pressure thresholds, and demand-supply alignment. The magnitude of the penalty factors influences how strictly these constraints are enforced during optimization and can affect the resulting optimal solution by prioritizing feasibility over performance. Therefore, the choice of penalty factors is problem-specific and can be fine-tuned to achieve an appropriate balance between constraint satisfaction and optimization performance. Note that if heat demand is the only source of uncertainty to be considered, then r_i represents a single realization of the demand profile. In that case, the augmented objective function takes the following form:

$$J(x, r_i) = M_{total}(x) + \mathscr{P}(x, r_i) \tag{6}$$

This formulation is efficient because the evaluation of emissions and

generated power is independent of heat demand. Additionally, it reduces computational time, as the simulation is performed for each proposed control setting, key performance indicators (KPIs) are retrieved, and the simulation output is evaluated using the defined augmented objective function. In this case, we assume that the heat demand (E_{demand}) is uncertain, with an expected value $\mathbb{E}(E_{demand})$ and a known variance. Consequently, the list of constraints remains unchanged, except for the demand-supply constraint, which is reformulated to account for the uncertain demand as follows:

$$E_{demand}(r_i) = \mathbb{E}(E_{demand}) + \widetilde{E}_{demand}(r_i) \tag{7}$$

3.3. Optimization algorithm

In this study, Genetic Algorithm (GA) was used for optimization. GA is a population-based optimization algorithm inspired by Darwin's theory of evolution and biological operators such as selection, crossover, and mutation. The process begins with a diverse set of randomly generated solutions, forming an initial population. The next step, known as reproduction and inheritance, involves individuals in the population producing offspring and passing on their characteristics through a process similar to genetic recombination. The algorithm evaluates each solution's fitness based on how well it solves the problem at hand. Solutions with higher fitness scores have a greater chance of being selected as parents for the next generation. This cycle of reproduction, inheritance, and selection repeats over multiple generations. With each iteration, the population tends to improve as fitter individuals are more likely to survive and pass on their traits [45,46].

The process terminates based on imposed conditions such as reaching a maximum number of generations, the highest fitness remaining unchanged in successive iterations, or manual termination. This approach allows GAs to efficiently explore large solution spaces and find globally optimal or near-optimal solutions, particularly in cases where traditional optimization methods may struggle due to complex or nonlinear problem landscapes [47].

The geothermal plant is modeled using an in-house developed solver [37]. A key characteristic of this modeling approach is its high accuracy. However, this comes with a limitation: the solver does not provide access to gradients. This restriction, in turn, limits the applicability of gradient-based algorithms, such as interior-point methods. To address this challenge, a meta-heuristic approach, such as the GA, can be employed. GA is a better choice in this context because it is gradient-free and has a strong capability to converge to a solution effectively. One of the main disadvantages of GA is the tuning of the optimizer parameters to ensure computational efficiency and convergence of the method. The GA optimization employed in this case study is based on the parameters in Table 2.

4. Results

In the first test, the results of the optimization under uncertainty for both objective functions for one fixed heat demand is shown. For this test, a fixed demand value of 6 MW is used, and the uncertainty is assumed with a standard deviation of 5 % from the nominal value. For all the cases in the result section, the realizations of uncertain demand are assumed to be equiprobable.

Table 2
Configuration and parameters of the GA optimization employed in the study.

Parameters/ Configuration	Value/Method
Objective function (for day-ahead)	Minimizing the expected value of the emission Maximizing the expected value of profit
Population size	50
Selection operation	Elitism
Cross over probabilities	70 %
Mutation probabilities	20 %
Mutation range	Based on a uniform distribution between the lower and upper bound specified for each gene
Maximum number of generations	100
Termination criteria	Maximum generation to be reached

The penalty factors used in the objective function (Equation (5)) were set to 1000, 100, and 10 for c_1, c_2, and c_3, respectively. The selection was through an iterative tuning process to ensure numerical stability and to appropriately enforce constraint violations. Although no formal sensitivity analysis was conducted, the chosen values were found to provide a suitable balance between penalizing constraint violations and allowing the optimizer to explore feasible solution spaces. The optimization algorithm enforces lower and upper bounds on all control variables (as stated in Equation (1)), defined as follows: $f^{esp} \in [30,70]$, $p_{wh}^{prod} \in [2,20]$, $q^{gas,grid} \in [0,100]$, $q^{s} \in [20,150]$, $u \in [0,100]$, $v \in [0,100]$.

Using genetic algorithm (GA), the optimization tracked the progression of fitness values across multiple generations, reflecting how well the system met each objective over time. Additionally, GA allowed for the evolution of six selected control variables, whose adjustments over generations reveal how different parameter combinations contribute to achieving the desired objectives. This analysis provides insights into the trade-offs between environmental and economic goals and highlights the control variables' role in balancing these objectives.

To present the initial results, a comparison for the fitness values and the evolution of control variables across generations for both objectives: minimizing emissions and maximizing profit are shown in Fig. 3. The impact of proposed control for both objective functions on the power generated from the geothermal doublet, plant and the net electricity power consumption is shown in Fig. 4. This result demonstrates that the algorithm effectively devised distinct control strategies tailored to each objective function. By optimizing separately for emission reduction and profit maximization, the GA was able to explore distinct control pathways that aligned with each objective, confirming its capability to adapt the control variables in response to varying optimization goals. The resulting emission for the emission minimization objective achieved a substantial reduction of 70 % compared to the emission of the profit maximization objective.

The reduction in emissions under the emission-focused objective was achieved primarily through reduced gas usage in the gas boiler, u value was to 53 % for the emission objective compared to 99.7 % for the profit objective function. By further analyzing the contribution to the produced power in Fig. 4, it can be seen that for the same plant power (to meet the uncertain heat demand), a higher production from geothermal doublet was proposed to minimize the emission. Higher profit objective leads to a higher utilization of the gas in the boiler which gives a higher emission. In a different observation, for the emission minimization objective, it can be observed that the net electricity consumption was turned to be positive, meaning that the fraction of the utilized gas in CHP could provide more electricity to the system than it is required which was sufficient for the produced geothermal power. By tracking these outcomes, we can illustrate how GA balances environmental and economic objectives and observe how each set of control variables adapts to prioritize emission reduction or profit maximization over successive generations.

Since the price can have an impact on the optimum operation (profit maximization or emission minimization) from the geothermal plant, a list of scenarios were performed by varying the prices aiming at optimizing the profit. These price ranges are used solely for sensitivity analysis to evaluate the effect of different pricing conditions, and are not intended to represent short-term fluctuating prices for gas, CO_2, or heat. For the scenarios a fixed heating demand of 6.0 MW was used. A total of 90 scenarios were performed by varying the prices in the following ranges, CO_2 [60–300] €/tonne, heat [20−100] €/GJ, and electricity [30–90] €/MWh. These scenarios were ran for a fixed assumed gas price (2.5 €/MMBtu). The results of different scenarios for profit

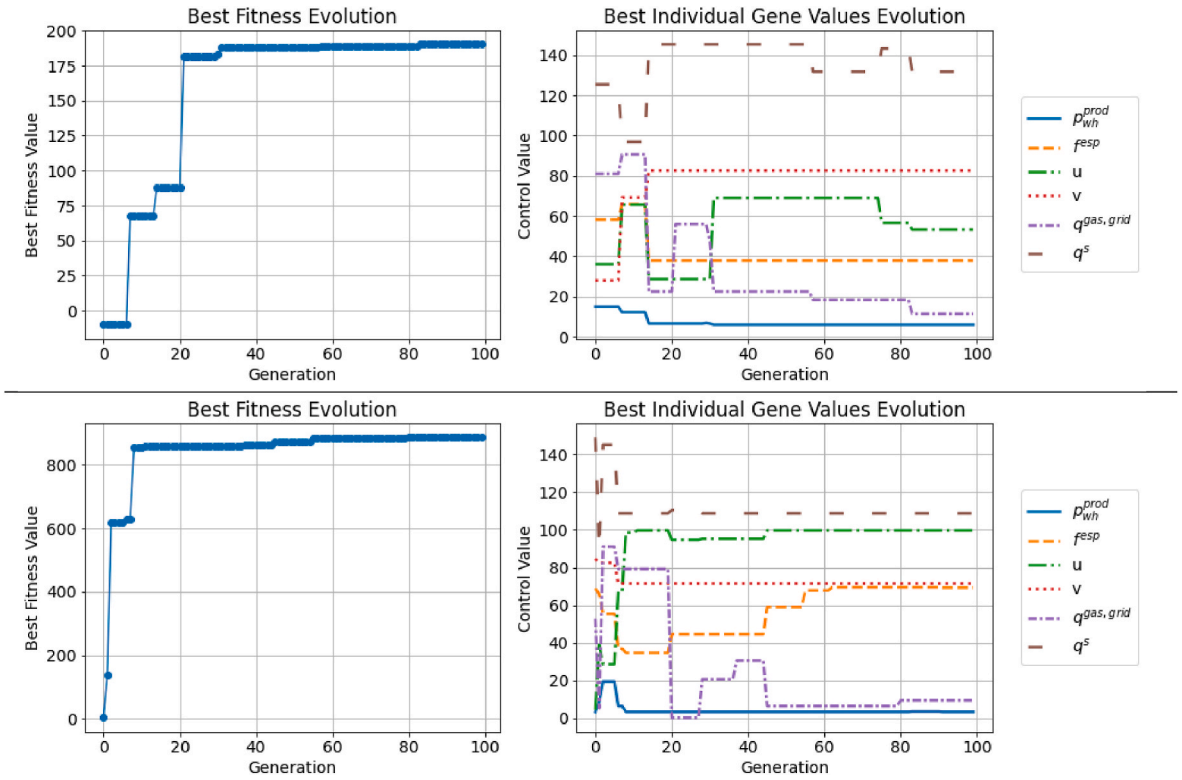

Fig. 3. Evolution of fitness values and control variables across generations for objectives of (top) minimizing total emissions and (bottom) maximizing profit. For profit maximization the following fixed prices were assumed c_{CO2}, = 60 €/tonne, c_{el} = 150 €/MWh, c_{heat} = 30 Euros €/GJ, and c_{gas} = 2.5 €/MMBtu.

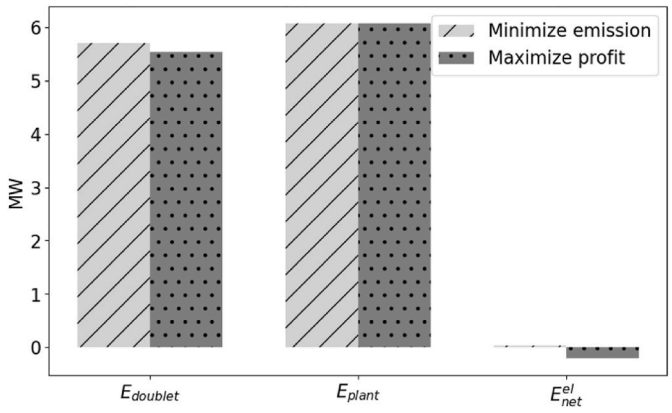

Fig. 4. Comparison of energy produced by the geothermal doublet ($E_{doublet}$), geothermal plant (E_{plant}), and the net electricity consumption (E_{net}^{el}) across two objective functions. The bars represent the respective values for each metric in MW; the objective functions were distinguished by different color and patterns.

maximization are shown in Fig. 5. The resulting emission from the profit maximization are shown in Fig. 6. The contour plots were made based on normalized profit, by considering the maximum profit made in all the optimized cases.

In the scenario analysis performed, a strong influence of heat price on profit maximization was observed. Scenarios with high electricity prices tended to yield higher profits, primarily because the optimal solution involved electricity production within the geothermal plant, generating a surplus beyond what was needed to sustain plant operations. Interestingly, CO_2 price showed a relatively low impact on profitability, suggesting that even with higher CO_2 costs, optimal solutions could still be achieved (Fig. 6). As previously described, high profits were associated with increased emissions which aligns with the contour plot of emissions for optimized profit cases.

The absence of a clear optimum point in the contour plot highlights the necessity for heuristic algorithms, such as GA, to effectively navigate the complex, multi-dimensional landscape of this optimization problem. It should be noted that these results are highly dependent on the specific plant configuration, pricing structure, and underlying properties, and no generic conclusions are intended.

The next problem was based on day-ahead production optimization with a prediction horizon of 24 h. Among the prices varied in the previous sensitivity analysis, only electricity has an hourly profile, which is incorporated in this section to reflect day-ahead market conditions. An example heating demand profile was generated with a maximum uncertainty of 5 % around the mean value of demand which is uniformly distributed (Fig. 7). The variability of the heating demand through the day was made in such a way that it corresponds to the heating demand in actual district heating grids [48]. It should be noted that such profiles, including both electricity prices and heat demand, can be influenced by weather conditions. While weather-driven prediction models are not considered in this paper, they can be readily integrated as boundary conditions or scenarios within the optimization framework. Both objective functions, targeting expected emission minimization and profit maximization, were evaluated on the same example of uncertain heating demand.

In other studies, heat demand is often modeled or forecasted using weather data and time-related features to improve the accuracy of operational planning [36]. Such forecasting-based approaches are valuable for proactive control but were not within the scope of this study, which focuses on optimizing control strategies based on given demand profiles. As earlier explained, the realizations in the uncertainty space of the heating demand are all treated to be equiprobable due to the choice of uniform distribution for the uncertainty. In this case, 50 realizations (24 h profile) were made which corresponds to a chance of 2 % for each profile to occur. The constraint to meet the heat demand at each hour, as a part of the augmented objective function, is still in place

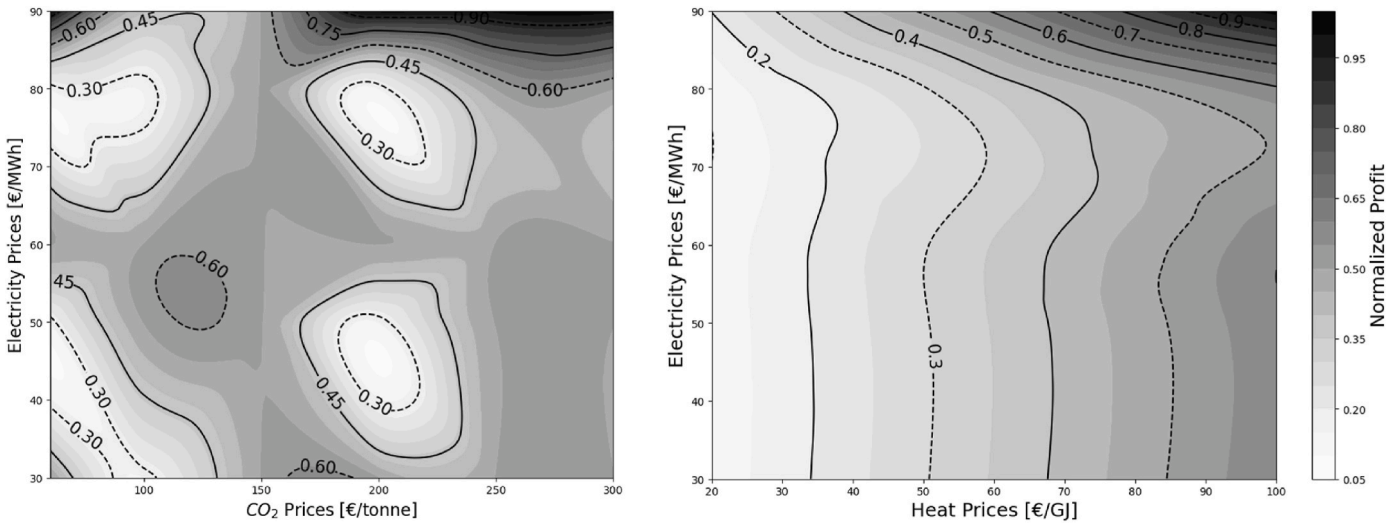

Fig. 5. 2D contour plot of optimum normalized profit based on scenarios varying CO_2, heat and electricity price for a fixed demand, in this case 6.0 MW. The left plot shows the impact of CO_2 and electricity price, and the right plot shows the impact of electricity and heat price.

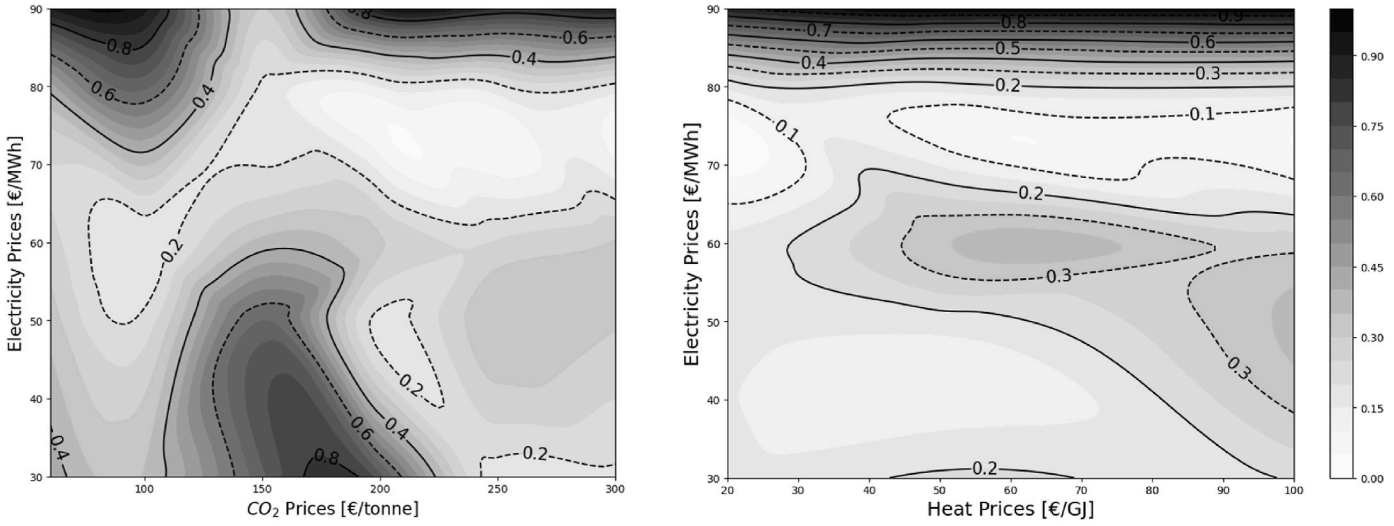

Fig. 6. 2D contour plot of optimum normalized emission based on scenarios varying CO_2, heat and electricity price for a fixed demand, in this case 6.0 MW. The left plot shows the impact of CO_2 and electricity price, and the right plot shows the impact of electricity and heat price.

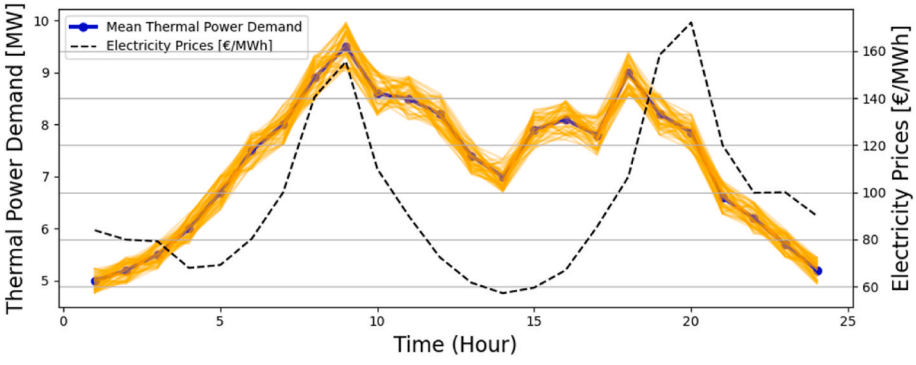

Fig. 7. Thermal power demand profile over time, mean and sampled demand values are plotted, based on 50 uniformly distributed random samples (yellow lines). (For interpretation of the references to color in this figure legend, the reader is referred to the Web version of this article.)

to prevent underproduction. For the maximization of profit, the heat, CO_2 and gas price during the next day was assumed to be constant with the values of 50 €/GJ, 100 €/tonne, and 2.5 €/MMBtu, respectively. An electricity profile price was assumed for the day-ahead market based on data obtained from market data available on EPEX SPOT and that is shown in Fig. 7.

The resulting control settings for all the control parameters for both optimization problems are shown in Fig. 8. The optimization results indicate a variation in control settings across the two objective functions examined. The optimized control variables, comparing the two optimization problems, exhibit only minor differences in the range that they were explored. The notable distinction can be found in the fraction u of the gas to the gas boiler and gas flow $q^{gas,grid}$ from the grid for the emission and profit objectives. For the case with minimizing emission, more gas is routed to CHP to produce electricity for the usage of the pumps in the geothermal plant, however for the profit maximization case study, the optimum settings were in a higher usage of the gas (both from the geothermal plant and grid) in the gas boiler for supplying the heat. It is important to note that the variation in the geothermal wellhead pressure of the production well and ESP frequency are coupled, and multiple combinations of these control variables can lead to the same production rate in the geothermal plant. To further improve the control algorithm and avoid this redundancy issue in the control settings, it is recommended to penalize the number of changes in the control parameters over the time horizon to avoid large step changes proposed by the optimization algorithm.

While the control strategy allows hourly updates, we acknowledge that rapid changes (such as those observed in Fig. 8) may not reflect the gradual control adjustments typically applied in practice. Such sudden load changes can impact the integrity of the equipment and lead to long-term reservoir challenges. In field applications, some control variables, such as ESP frequency, are often adjusted progressively over a longer period rather than through sudden changes, depending on the manufacturer's specifications and the amplitude of the change. Although dynamic system constraints are not explicitly modeled in this study, they can be incorporated in future work to reflect more realistic operational behavior.

The total day-ahead emission for the case of maximizing the profit leads to a significantly higher emission, see Fig. 9, by 87.5 % increase mainly driven by the higher utilization of the gas from the geothermal brine and grid. For the profit objective, the optimum control that minimizes emissions will lead to a 2.7 % lower profit compared to the control settings leading to the maximum profit. Since the majority of the supplied heat is provided by the geothermal plant, the impact of minimizing emission on the profit generated during the operation is minute.

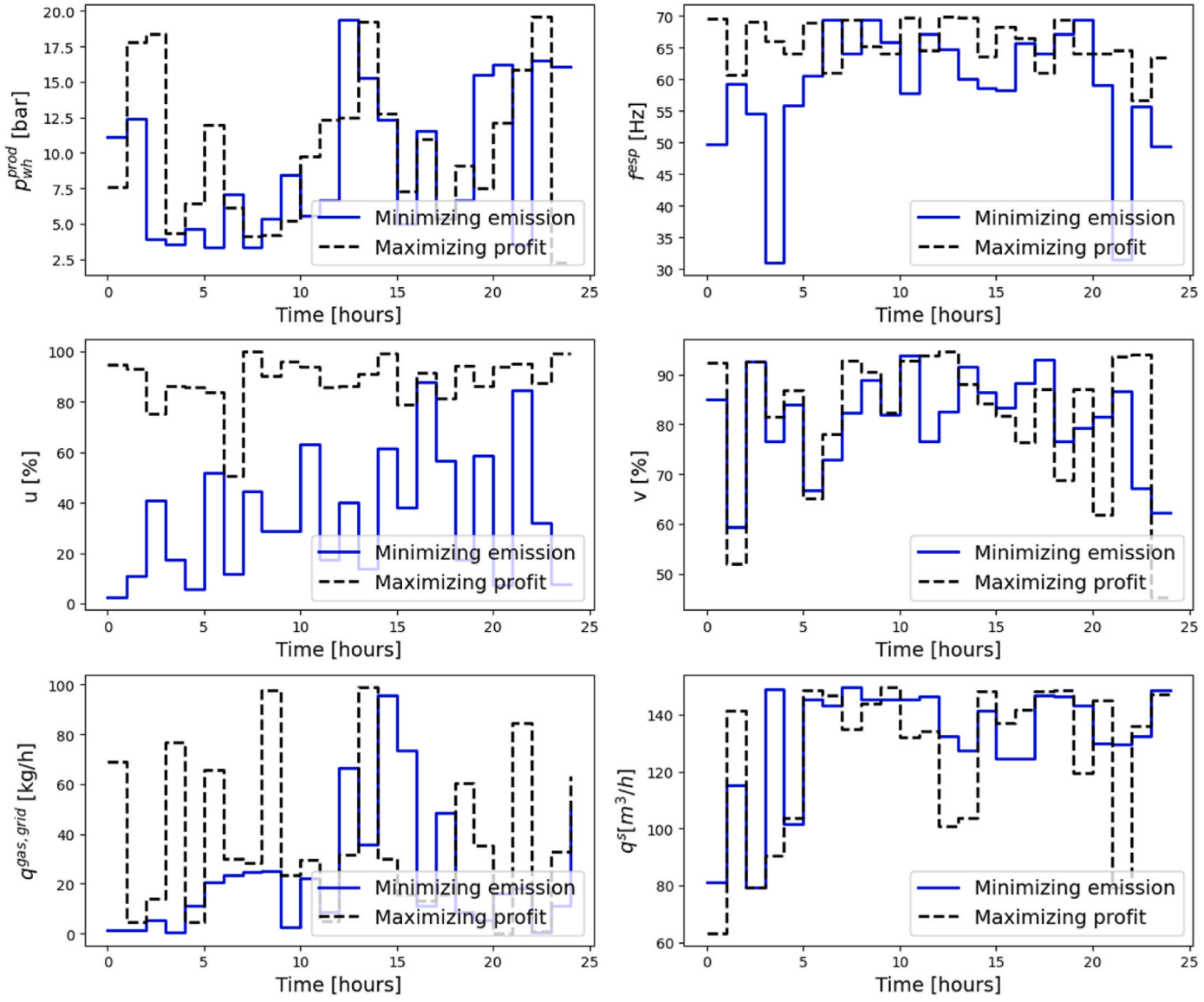

Fig. 8. Optimal control settings for all the control variables, including wellhead pressure of the geothermal production well, ESP frequency, fraction of the gas to the boiler (u), fraction of the water to the heat exchanger (v), gas flow rate from the grid, and the flow rate of the water in the secondary loop, for both emission minimization and profit maximization objective function.

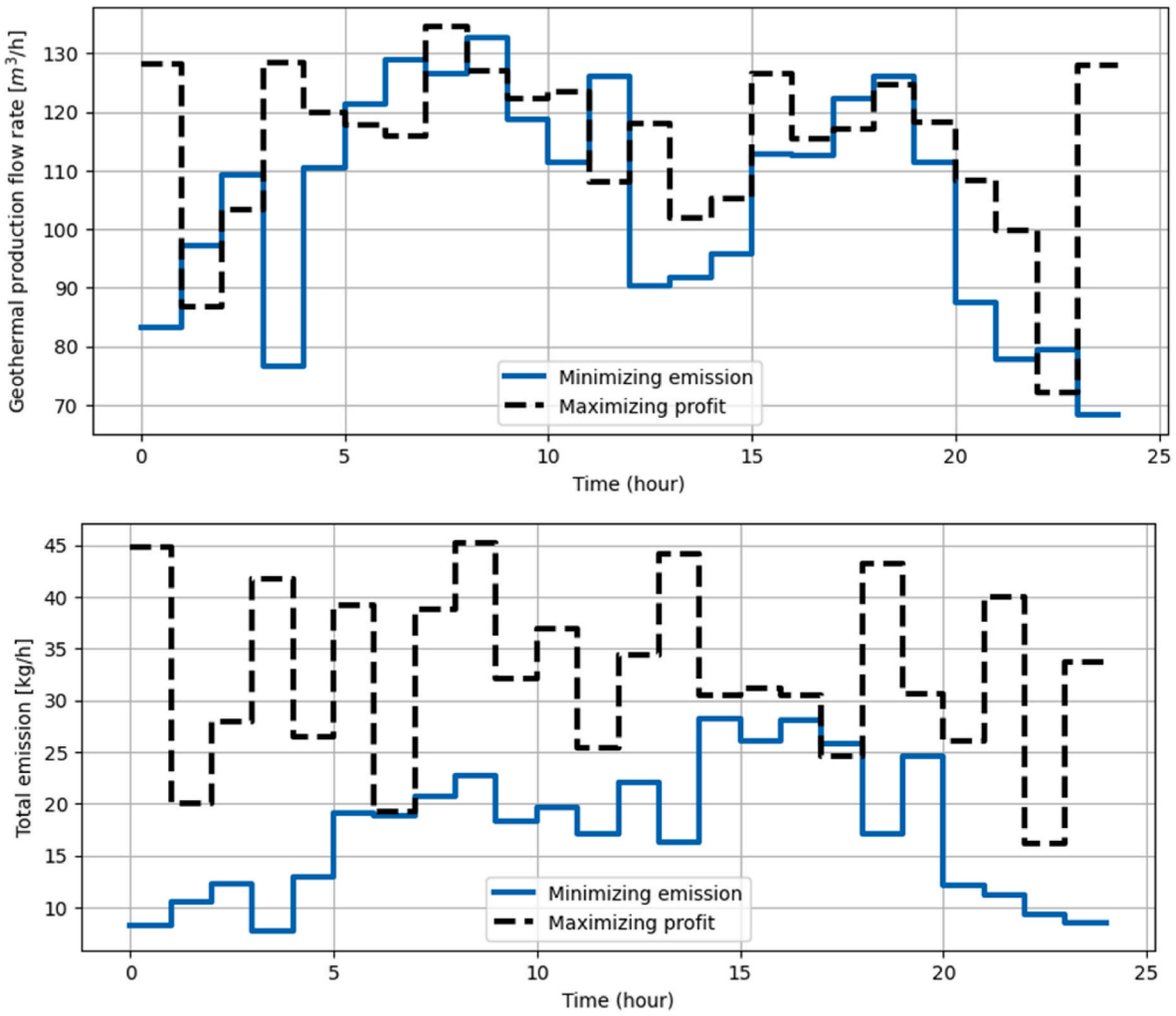

Fig. 9. The hourly (top) geothermal production rate and (bottom) total CO_2 emission for the day-ahead production optimization shown for minimizing emission and maximizing profit case study.

It is shown in Fig. 9 that the contribution of the geothermal well production for both objective functions remains high and not significantly changed, and the main components that are impacted to achieve the desired objectives are the utilization of the gas from the grid and electricity production in CHP. It should be noted that the results in this section depend on the gas, CO_2, heat and electricity price chosen in the profit objective function.

Robust optimization is proposed as a rigorous approach to ensure optimal control for a geothermal plant under heat demand uncertainty. In order to demonstrate the added value of robust optimization, its solution x^{opt} is compared to the solutions $x_i^{opt}, i = 1, \ldots, 50,$ of the deterministic optimization performed on every individual realization (total of 50) from the uncertainty space. Under the assumption of equiprobable realizations, the optimal control solution x^{opt} that performs well across all realizations was achieved by optimizing the expected objective function. In Fig. 10 the expected objective function values $\overline{J}(x_i^{opt}), i = 1, \ldots, 50$ are shown together with $\overline{J}(x^{opt})$ with $\overline{J}$ the averaged (over the realizations) emission. As expected, the robust optimization approach led to the best overall performance in terms of expected objective function improvement, that is, $\overline{J}(x^{opt}) \leq \overline{J}(x_i^{opt}), i = 1, \ldots, 50$. The figure shows also that control obtained through deterministic optimization may result in a much higher expected objective function value indicating an inferior performance for other realizations. Similar observation can be made for the case of maximizing profits of which the results are shown in Fig. 10 b). In conclusion, the control strategies obtained by robust optimization for both objective functions, show more resilient and robust performance across all considered realization of uncertain heat demand, whereas deterministic optimization can perform poorly for certain realizations, as implied by Fig. 10. For the emission minimization the objective function of robust optimization was found to be 191.5 while the best realization led to the objective function of 180.2 in which the robust optimization has a 5.9 % improvement in the objective function, demonstrating its effectiveness in handling the uncertainties inherent in geothermal plant control. For the profit maximization, only a minute increase of 1.4 % was found for the robust optimization compared to the best of all the realizations. However, we emphasize that even though in the latter case the increase is small performing deterministic optimizations for all realizations and taking the control that results in highest expectation objective function value is not a reliable substitute of the robust optimization approach.

5. Conclusions

Uncertainties in various parameters and processes of geothermal energy production can significantly impact the optimal control of geothermal plants. These uncertainties, arising from diverse sources and varying over time, necessitate a systematic approach to integrate them into the operational decision-making processes of geothermal plants. This paper introduces a novel stochastic optimization-based control policy designed to optimize the operation of geothermal plants under

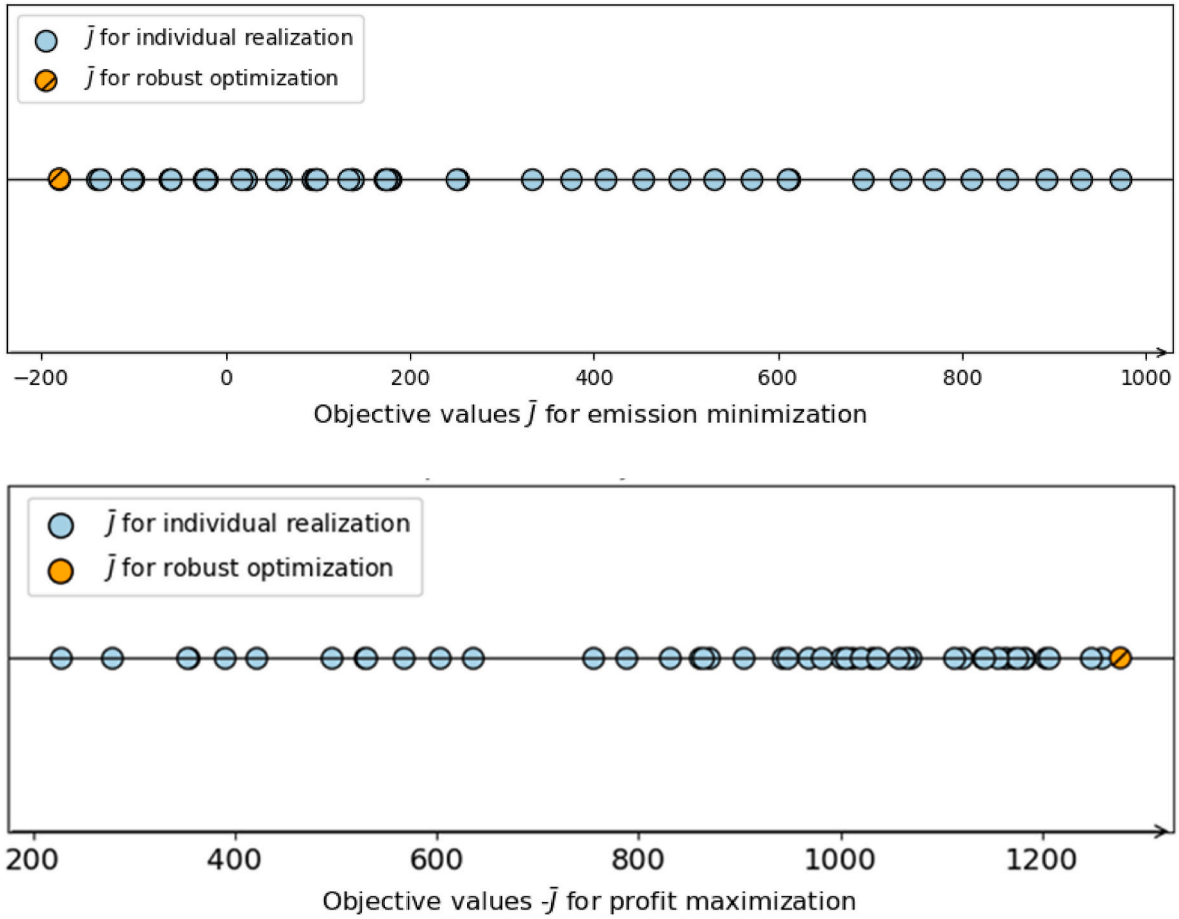

Fig. 10. Comparison of the expected objective function value from the robust optimization result with the deterministic solutions for all the realizations for (top) emission minimization and (bottom) profit maximization objectives.

heating demand uncertainty. The proposed stochastic optimization framework aims to optimize the expected objective function across all scenarios. In an ex-post analysis, the optimal policy for the worst-case realization is determined, yielding a robust solution. When the worst-case scenario policy is applied universally across all scenarios, it results in a solution that is more conservative and risk averse. Despite its reduced efficiency, the robust solution is chosen as the preferred control policy due to its enhanced reliability under uncertainty.

The optimization method supports several critical control and operational parameters in the plant, including geothermal wellhead pressure, electric submersible pump frequency (which impacts the production rate of geothermal wells), the distribution of gas to the boiler and combined heat and power units, the allocation of liquid to the heat exchanger, the flow rate of gas from the grid (to address demand-supply mismatches), and the flow rate of the secondary fluid connected to the heat demand. A Genetic Algorithm was employed to solve the optimization problem, incorporating two objective functions: minimizing emissions and maximizing profit. Operational constraints were integrated into the framework by penalizing violations in the objective function.

The results demonstrated the robustness and effectiveness of the proposed optimization approach in managing geothermal plant operations. The robust optimization method provided a control strategy capable of performing well across all uncertainty realizations. Conversely, deterministic optimization, which does not account for uncertainties, was shown to lead to suboptimal operation. Optimizing control based on a single realization resulted in inferior solutions for other scenarios, highlighting the importance of incorporating uncertainties into the optimization process.

While the proposed approach offers a robust methodology for addressing uncertainties in geothermal plant operations, a more comprehensive case study would be required to fully explore its potential. For example, uncertainties related to fluid composition and equipment degradation, which can significantly influence optimal control settings, were not included in the current formulation. Additionally, the anticipated increase in electrification of energy infrastructure, including the adoption of heat pumps and its interplay with electricity pricing, represents a critical area for future investigation.

To further enhance the practicality of the proposed workflow, future work should focus on improving the computational efficiency of the optimizer. This could involve incorporating gradient-based optimization methods or exploring alternative strategies, such as adaptive mutation techniques (e.g., Ref. [49]), to enable real-time production optimization. For future work, transient models to simulate the dynamic response and behavior of the system can be implemented and additional constraints can be introduced to limit the load changes in the system and the magnitude of control actions, such as variations in ESP frequency and wellhead pressures, to further align with operational practices. Geothermal energy has a low environmental footprint; however, in reservoirs with accompanying gases, CO_2 emissions may occur during production. Research on CO_2-neutral gas utilization [50] and its impact on optimal operational strategies can be further studied. Finally, the validation of the proposed control strategies on field cases is recommended for future studies.

CRediT authorship contribution statement

Pejman Shoeibi Omrani: Writing – review & editing, Writing –

original draft, Visualization, Validation, Software, Methodology, Investigation, Formal analysis, Data curation, Conceptualization. **Paul J.P. Egberts:** Writing – review & editing, Software, Methodology, Investigation. **Huub H.M. Rijnaarts:** Writing – review & editing, Supervision. **Shahab Shariat Torbaghan:** Writing – review & editing, Supervision, Methodology.

Data and materials availability

Data will be made available upon reasonable request.

Ethics approval, consent to participate, and consent to publish declarations

Not applicable.

Declaration of competing interest

The authors declare that they have no known competing financial interests or personal relationships that could have appeared to influence the work reported in this paper.

Nomenclature

Symbol	
c_1, c_2, c_3	Penalty factors for constraints' violation [−]
c_{CO_2}	Price of CO_2 [€/tonne]
c_{el}	Price of the electricity [€/MWh]
c_{gas}	Price of the gas from the grid [€/MMBtu]
c_{heat}	Price of the heat [€/GJ]
C_{total}	Total profit [€]
C_w	Specific heat capacity of water [J/(kg.K)]
E_{demand}	Thermal energy demand [MW]
E_{plant}	Thermal power generated by the plant [MW]
E_{total}	The net generated thermal power subtracting the power consumption [MW]
E_{net}^{el}	Electricity surplus [MW]
M	CO_2 emission [kg/s of CO_2 equivalent]
p	Pressure [bar]
$\mathscr{P}$	Penalty term for constraint violation
q	Fluid flow rate [m^3/s]
T	Temperature [C]
u	Gas flow fraction [−]
v	Water flow fraction in the secondary system [−]
x	Control vector
Abbreviations	
CHP	Combined heat and power
ESP	Electrical Submersible Pump
GA	Genetic Algorithm
PI	Productivity Index
SBSO	Scenario-based Stochastic Optimization
VLP	Vertical lift performance
Superscript	
el	Electric power
geo	Geothermal production in the primary system
gas,geo	Gas from the geothermal doublet
gas, grid	Gas from the grid
p	Primary system
s	Secondary system
Subscript	
boosterpump	Booster pump on the geothermal injection side (primary system)
in	Inlet (refers to any component)
net	Net power generated/consumed
out	Outlet (refers to any component)
w	Water
wh	wellhead

Annex 1. Modelling approach for the geothermal plant

The equations for the different components of the geothermal plant are described in this section.

VLP-IPR relation

For solving the rate of the producer well incorporating an ESP, a procedure known as nodal analysis needs to be performed. The geothermal production is a pressure-driven system and the pressure on several nodes of the system together with the resistance between the nodes will determine the production rate. The system consists of five pressure nodes from subsurface to surface: P_{res} (reservoir pressure), P_{bh} (bottomhole pressure), $P_{esp,in}$ (suction pressure of ESP), $P_{esp,out}$ (discharge pressure of ESP) and P_{wh} (wellhead pressure).

The inflow performance relation is used to relate two of the pressure nodes, P_{res} and P_{bh} given a production rate q using a linear relation using the productivity index (PI)

$$q^p = PI \cdot (P_{\mathrm{res}} - P_{\mathrm{bh}}) \tag{8}$$

Given the wellhead pressure P_{wh} and a production rate q^p, the vertical lift performance curves of the upper (above the ESP) and lower part of the well and the ESP pressure drop the bottomhole pressure P_{bh} can be derived. The nodal analysis calculates the flowrate q^p so that the P_{bh} of the well calculation and the inflow performance relation is equal. Its solution is denoted by q^p ,with superscript p to refer to the primary system, see Fig. 1.

Due to different pipe diameters in the completion, the pressure drop equation needs to be integrated over the full length of the pipe. The vertical lift performance (VLP) estimation in the producer well is divided into two sections, upstream (from bottomhole to the inlet of ESP) and downstream (from discharge of ESP to wellhead) of the ESP. The pressure drop equation is as follows

$$\frac{dP}{dl} = \left(g\sin(\theta) + \frac{f_c}{2D_h}|u_m|u_m\right)(\alpha_g\rho_g + \alpha_l\rho_l) - \alpha_g\rho_g u_g\frac{du_g}{dx} - \alpha_l\rho_l u_l\frac{du_l}{dx}, \tag{9}$$

In which l is the length along the tubing or pipe, D_h is the hydraulic diameter of the pipe, θ is the inclination of the pipe, and g is gravitational acceleration. In the formulation, the hold-up is denoted as α, density as ρ and superficial velocity as u, with the subscripts g and l stands for gas and liquid phase. Since, multiphase flow in the production tubing or casing is expected, mixture velocity (u_m) is used for the pressure drop calculations, which is defined as

$$u_m = \alpha_g u_g + \alpha_l u_l \tag{10}$$

The friction coefficient (f_c) used for the pressure drop calculation is [51]:

$$f_c = \left[1.14 - 2\,log\left(\frac{\varepsilon}{D_h} + \frac{21.25}{Re^{0.9}}\right)\right]^{-2} \tag{11}$$

where ε is the tubing/casing roughness and Re is the Reynolds number.

The ESP hydraulic performance model is a fit function to the suppliers' provided pump curves from which the ESP head can be estimated based on the production rate and pump frequency f_{esp}:

$$\Delta p = \left(p_{esp,out} - p_{esp,in}\right) = F\left(q^p, f_{esp}\right) \tag{12}$$

Heat exchanger

The heat exchanger model describes the relationship between the input and output temperatures of the primary and secondary fluid streams, based on flow rates and heat transfer dynamics. Mathematically, the model is expressed by a function F_{hex}: $T^p_{out}, T^s_{out} = F_{hex}\left(T^p_{in}, T^s_{in}, q^p, q^s, v\right)$. The output temperatures depend on the input temperatures, flow rates of the primary (q^p) and secondary (vq^s) systems, and heat transfer coefficient. The output temperatures are given by

$$T^p_{out} = T^p_{in} - \frac{h}{C_w q^p}, T^s_{out} = T^s_{in} + \frac{h}{C_w v q^s} \tag{13}$$

where $h = e\,h_{max}$ represents the heat transfer rate, and $h_{max} = c_{min}\left|T^p_{in} - T^s_{in}\right|$ is the maximum possible heat transfer. The effectiveness, ϵ, depends on the configuration of the heat exchanger, parallel or counterflow which is calculated using the following formulas, respectively:

- For parallel flow:

$$\epsilon = \frac{1 - e^{-NTU(1+c_r)}}{1 + c_r} \tag{14}$$

- For counter plate

$$\epsilon = \begin{cases} \dfrac{NTU}{1+NTU}, \text{if } c_r = 1 \\ 1 - e^{-NTU}, \text{if } c_r < 0.01 \\ \dfrac{1 - e^{-NTU(1+c_r)}}{1 - c_r e^{-NTU(1+c_r)}}, \text{otherwise} \end{cases} \tag{15}$$

Here the key parameters are: $NTU = H/c_{min}$, $c_r = c_{min}/c_{max}$, $c^p = \rho q^p C_w$, $c^s = \rho v q^s C_w$, $c_{max} = \max(c^p, c^s)$, $c_{min} = \min(c^p, c^s)$

where H is the heat transfer coefficient and C_w is the specific heat capacity of water. This model effectively captures the thermodynamic behavior of the heat exchanger, accounting for heat transfer limitations, flow rate effects, and configuration-specific performance through the non-dimensional effectiveness (ϵ) and number of transfer units (NTU). It provides a robust framework for analyzing and optimizing heat exchanger performance in both parallel and counterflow configurations.

Gas boiler

The gas boiler model describes its role in delivering higher temperatures when a geothermal doublet is insufficient. The relationship governing the

gas boiler is expressed as

$$T_{blr,out}, M_{blr} = F_{blr}\left(T_{blr,in}, q^p, q^s, u, v\right), \tag{16}$$

where $T_{blr,in} = T_{hex,out}$. The outlet temperature of the gas boiler is given by

$$T_{blr,out} = T_{blr,in} + \frac{E_{boiler}}{C_w v \rho q^s} \tag{17}$$

Here E_{boiler} is the thermal power provided by the boiler, calculated as

$$E_{boiler} = \eta_{blr} Huq_{gas}, \tag{18}$$

with the following definitions.

- η_{blr}: the efficiency factor of the gas boiler (typically $\eta_{blr} = 0.8$),
- H: calorific value of the gas ≈ 50 MJ/m^3
- q_{gas} : gas flow rate ($[m^3/s]$) ,
- $u \in [0, 1]$: gas flow fraction

The CO_2 emission, M_{blr} [kg/s], from the gas boiler is given by

$$M_{blr} = e_{gas}\, Huq_{gas} \tag{19}$$

with e_{gas} [kg/J] is the gas emission factor. This model captures the thermodynamic and environmental behavior of the gas boiler, accounting for its efficiency, thermal power output, and emissions. It ensures accurate modeling of the boiler's contribution to heat delivery, as well as the associated fuel consumption and CO_2 emissions. The integration of parameters such as the calorific value (H) and gas flow fraction (u) allows for the flexible operation of the boiler while maintaining realistic energy and environmental constraints.

CHP (combined heat and power)

The CHP model describes its ability to simultaneously generate heat and electricity using natural gas as a fuel source. The governing relationship for the CHP system is given as:

$$T_{chp,out}, E_{chp}, M_{chp} = F_{chp}\left(T_{chp,in}, q_{gas}, q^s, u, v\right), \tag{20}$$

with $T_{chp,in} = T^s_{in}$. The total generated power P_{chp} produced by the CHP can be written as:

$$P_{chp} = \eta_{chp} H (1-u) q_{gas}, \tag{21}$$

with a typical efficiency of $\eta_{chp} = 0.8$. In order to calculate the generated heat and electricity from the CHP the following assumption was used; $E^{el}_{chp} = \frac{1}{3} P_{chp}$ the power for electricity, $E_{chp} = \frac{2}{3} P_{chp}$ the power for the heat. The outlet temperature of the CHP is calculated as:

$$T_{chp,out} = T_{chp,in} + \frac{E_{chp}}{C_w (1-v) \rho q^s} \tag{22}$$

The CO_2 emission, M_{chp} [kg/s], from the CHP system is given by

$$M_{chp} = e_{gas}\, H\, (1-u)\, q_{gas} \tag{23}$$

with e_{gas} [kg/J] being the gas emission factor. This model effectively captures the thermodynamic and environmental characteristics of the CHP system, detailing its ability to convert natural gas into both thermal energy and electricity with a defined efficiency. The integration of key parameters such as gas flow fraction (u) and flow rates ensure accurate modeling of its operational performance and associated CO_2 emissions. By separating power generation into heat and electricity components, the model provides a detailed framework for optimizing CHP utilization in energy systems.

ESP

This model is built upon manufacturer-provided correlations that relate the pump head, $\Delta p = \left(p_{esp,in} - p_{esp,out}\right)$, to the flowrate q^p and pump frequency f_{esp}. The correlations are often found in the pump curves and enable the prediction of pump performance under varying operating conditions. The relationship was fitted by using a polynomial regression calibrated on pump curve data.

The required pump power, E^{el}_{esp} [W], is calculated as:

$$E^{el}_{esp} = \frac{q^p \Delta p.}{\eta_{esp}}, \tag{24}$$

where a typical efficiency of the ESP is assumed to be $\eta_{esp} = 0.65$. This relation highlights the dependence of pump power requirement on the operational settings and efficiency, as defined by the pump performance curves.

The CO_2 emission, M_{esp} [kg/s], is given by

$$M_{esp} = e_{el}\, E^{el}_{esp} \tag{25}$$

with e_{el} [kg/J] the electricity emission factor. In case electric power from the CHP is used for the ESP then the CO_2 emission must be corrected:

$$M_{esp} = e_{el}\left(E^{el}_{esp} - \min\left(E^{el}_{chp}, E^{el}_{esp}\right)\right) \tag{26}$$

Booster pump

The required pump power $E^{el}_{boosterpump}$ [W]:

$$E^{el}_{boosterpump} = \frac{q^p \Delta p}{\eta_{bpump}}, \Delta p = \left(p_{bpump,in} - p_{bpump,out}\right) \tag{27}$$

The emission $M_{boosterpump}$ [kg/s]:

$$M_{boosterpump} = e_{el}\, E^{el}_{boosterpump} \tag{28}$$

with e_{el} [kg/J] the electricity emission factor for the pump power consumption.

References

[1] IEA, Geothermal Power, IEA, Paris, 2021. https://www.iea.org/reports/geothermal-power.
[2] G. Goetzl, D. Milenic, C. Schiflechner, Geothermal-DHC, European research network on geothermal energy in heating and cooling networks. Proceedings World Geothermal Congress 2020+1, Reykjavik, Iceland, 2021.
[3] G. Goetzl, J. Chicco, C. Schifflechner, J. Figueira, G. Tsironis, A. Zajacs, Pathways to better integrate geothermal energy at its full technological scale in European heating and cooling networks, Eur. Geol. 54 (2022).
[4] L. Wasch, R. Creusen, F. Eichinger, T. Goldberg, C. Kjoller, S. Regenspurg, T. Mathiesen, P. Shoeibi Omrani, V. van Pul-Verboom, Improving geothermal system performance through collective knowledge building and technology development, in: European Geothermal Congress 2019, 2019.
[5] J.D.D. Ocampo-Díaz, B. Valdez-Salaz, M. Shorr, M.I. Sauceda, N. Rosas-González, Review of corrosion and scaling problems in cerro prieto geothermal field over 31 years of commercial operations, in: Proceedings of the World Geothermal Congress 2005, vol. 1, 2005. Antalya, Türkiye, 24-29 April 2005.
[6] D.O. Schulte, D. Arnold, S. Geiger, V. Demyanov, I. Sass, Multi-objective optimization under uncertainty of geothermal reservoirs using experimental design-based proxy models, Geothermics 86 (2020) 101792, https://doi.org/10.1016/j.geothermics.2019.101792.
[7] H. Hoteit, X. He, B. Yan, V. Vahrenkamp, Uncertainty quantification and optimization method applied to time-continuous geothermal energy extraction, Geothermics 110 (2023) 102675.
[8] I.S. Moeck, Catalog of geothermal play types based on geologic controls, Renew. Sustain. Energy Rev. 37 (2014) 867–882.
[9] J. Poort, P. Shoeibi Omrani, L. Wasch, A. Twerda, H. de Zwart, Impact of geochemical uncertainties on geothermal fluid production and scaling precipitation in geothermal plants and facilities. Proceeding of European Geothermal Congress 2022, 2023. Berlin, Germany.
[10] K. Kieling, S. Regenspurg, L. André, C. Boeije, D. Clark, M.M. Demir, L. Wasch, The H2020 project REFLECT–Redefining fluid properties at extreme conditions to optimise future geothermal energy extraction, Eur. Geol. (54) (2022).
[11] J.W. Lund, P.J. Lienau, Geothermal district heating projects, in: International geothermal days, conference and summer school, 2009 2009. Slovakia.
[12] M.H. Shamsi, U. Ali, E. Mangina, J. O'Donnell, A framework for uncertainty quantification in building heat demand simulations using reduced-order grey-box energy models, Appl. Energy 275 (2020) 115141.
[13] M.H. Shamsi, U. Ali, E. Mangina, J. O'Donnell, Feature assessment frameworks to evaluate reduced-order grey-box building energy models, Appl. Energy 298 (2021) 117174.
[14] O. Özkaraca, A review of usage of optimization methods in geothermal power generation, Mugla J. Sci. Technol. 4 (2018) 130–136, https://doi.org/10.22531/muglajsci.437340.
[15] R.M.M. Fonseca, O. Leeuwenburgh, E. Della Rossa, P.M. Van den Hof, J.D. D. Jansen, Ensemble-based multiobjective optimization of on/off control devices under geological uncertainty, SPE Reservoir Eval. Eng. 18 (4) (2015) 554–563.
[16] N. Janatian, R. Sharma, A robust model predictive control with constraint modification for gas lift allocation optimization, J. Process Control 128 (2023) 102996.
[17] J.R. Patterson, M. Cardiff, K.L. Feigl, Optimizing geothermal production in fractured rock reservoirs under uncertainty, Geothermics 88 (2020). Article 101906.
[18] S. Jalilinasrabady, R. Itoi, P. Valdimarsson, G. Saevarsdottir, H. Fujii, Flash cycle optimization of Sabalan geothermal power plant employing exergy concept, Geothermics 43 (2012) 75–82.
[19] A. Bolatturk Coskun, M. Kanoglu, Thermodynamic and economic analysis and optimization of power cycles for a medium temperature geothermal resource, Energy Convers. Manag. 78 (2014) 39–49.
[20] X. Wang, X. Liu, C. Zhang, Parametric optimization and range analysis of organic rankine cycle for binary-cycle geothermal plant, Energy Convers. Manag. 80 (2014) 256–265.
[21] M.H. Aghagol, R. Hamidi, M.R. Heyhat, Assess the potential of geothermal resources using fuzzy logic and binary index overlay (case study: south Khorasan province, eastern Iran)", J. Tethys 4 (3) (2016) 221–241.
[22] H. Saffari, S. Sadeghi, M. Khoshzat, P. Mehregan, Thermodynamic analysis and optimization of a geothermal Kalina cycle system using artificial bee colony algorithm, Renew. Energy 89 (2016) 154–167.
[23] M. Pollet, L. Gosselin, J. Dallaire, F. Mathieu-Potvin, Optimization of geothermal power plant design for evolving operating conditions, Appl. Therm. Eng. 134 (2018) 118–129.
[24] F. Casella, Modeling, simulation, control, and optimization of a geothermal power plant, IEEE Trans. Energy Convers. 19 (1) (2004) 170–178.
[25] Yabanova, A. Keçebaş, "Development of ANN model for geothermal district heating system and a novel PIDbased control strategy", Appl. Therm. Eng. 51 (2013) 908–916.
[26] H. Ghasemi, M. Paci, A. Tizzanini, A. Mitsos, Modeling and optimization of a binary geothermal power plant, Energy 50 (2013) 412–428.
[27] D. Cupeiro Figueroa, D. Picard, L. Helsen, Short-term modeling of hybrid geothermal systems for model predictive control, Energy Build. 215 (2020), https://doi.org/10.1016/j.enbuild.2020.109884. Article 109884.
[28] M. Imran, R. Pili, M. Usman, F. Haglind, Dynamic modeling and control strategies of organic rankine cycle systems: methods and challenges, Appl. Energy 276 (2020) 115537.
[29] G. Cetin, O. Ozkaraca, A. Kecebas, Development of PID based control strategy in maximum exergy efficiency of a geothermal power plant, Renew. Sustain. Energy Rev. 137 (2021) 110623, https://doi.org/10.1016/j.rser.2020.110623.
[30] G. Cetin, A. Keçebaş, Optimization of thermodynamic performance with simulated annealing algorithm: a geothermal power plant, Renew. Energy 172 (2021) 968–982, https://doi.org/10.1016/j.renene.2021.03.101.
[31] W. Ling, Y. Liu, R. Young, T.T. Cladouhos, B. Jafarpour, Efficient data-driven models for prediction and optimization of geothermal power plant operations, Geothermics 119 (2024) 102924, https://doi.org/10.1016/j.geothermics.2024.102924.
[32] R. Adiga, Optimizing Geothermal Well Planning Under Reservoir Uncertainty with Stochastic Programming (Phd Thesis), The University of Auckland, 2023.
[33] M. Chen, A.F.B. Tompson, R.J. Mellors, O. Abdalla, An efficient optimization of well placement and control for a geothermal prospect under geological uncertainty, Appl. Energy 137 (2015) 352–363.
[34] A. Daniilidis, B. Alpsoy, R. Herber, Impact of technical and economic uncertainties on the economic performance of a deep geothermal heat system, Renew. Energy 114 (Part B) (2017) 805–816.
[35] S.P. Szklarz, E.G.D. Barros, N. Khoshnevis Gargar, S.H.J. Peeters, J.D. van Wees, V. van Pul-Verboom, Geothermal field development optimization under geomechanical constraints and geological uncertainty: application to a reservoir with stacked formations, Geothermics 123 (2024) 103094.
[36] M. Irl, J. Lambert, C. Wieland, H. Spliethoff, Development of an operational planning tool for geothermal plants with heat and power production, ASME. J. Energy Resour. Technol. 142 (9) (2020) 090903, https://doi.org/10.1115/1.4047755.
[37] P. Shoeibi Omrani, P.J.P. Egberts, R. Octaviano, Real-time monitoring and optimization of geothermal plants, GRC Trans. 46 (2022) (2022).
[38] R.P. Cosmo, F.A.R. Pereira, E.J. Soares, E.G. Ferreira, Addressing the root cause of calcite precipitation that leads to energy loss in geothermal systems, Geothermics 98 (2022) 102272.
[39] J.D. Jansen, Nodal Analysis of Oil and Gas Production Systems, Publisher: Society of Petroleum Engineers, 2017.
[40] A.J. Conejo, M. Carrión, J.M. Morales, Decision Making Under Uncertainty in Electricity Markets, vol. 1, Springer, New York, 2010, pp. 376–384.
[41] W.B. Powell, From reinforcement learning to optimal control: a unified framework for sequential decisions, in: Handbook of Reinforcement Learning and Control, Springer International Publishing, Cham, 2021, pp. 29–74.
[42] V. Gabrel, C. Murat, A. Thiele, Recent advances in robust optimization: an overview, Eur. J. Oper. Res. 235 (3) (2014) 471–483.
[43] P. Egberts, C. Tümer, K. Loh, R. Octaviano, Challenges in heat network design optimization, Energy 203 (2020) 117688.

[44] D. Krishnamoorthy, B. Foss, S. Skogestad, Real-time optimization under uncertainty applied to a gas lifted well network, Processes 4 (52) (2016).
[45] S.N. Sivanandam, S.N. Deepa, S.N. Sivanandam, S.N. Deepa, Genetic Algorithms, Springer Berlin Heidelberg, 2008, pp. 15–37.
[46] B.H. Sumida, A.I. Houston, J.M. McNamara, W.D. Hamilton, Genetic algorithms and evolution, J. Theor. Biol. 147 (1) (1990) 59–84.
[47] S. Mishra, S. Sahoo, M. Das, Genetic algorithm: an efficient tool for global optimization, Adv. Comput. Sci. Technol. 10 (8) (2017) 2201–2211.
[48] F.G.H. Koene, E.F. Matthijssen, M. Menkveld, Generating heat demand profiles of neighbourhoods, IOP Conf. Ser. Earth Environ. Sci. 1085 (2022) 012008.
[49] S. Uyar, S. Sariel, G. Eryigit, A gene based adaptive mutation strategy for genetic algorithms, in: K. Deb (Ed.), Genetic and Evolutionary Computation – GECCO 2004. GECCO 2004, Lecture Notes in Computer Science, vol 3103, Springer, Berlin, Heidelberg, 2004.
[50] C. Wieland, H. Spliethoff, T. Baumann, CO_2-neutral co-produced gas utilization for deep geothermal applications, Geothermics 88 (2020) 101895.
[51] D. Beggs, J. Brill, A study of two-phase flow in inclined pipes, Petrol. Technol. 25 (1973) 607–617.